INL/JOU-20-57168-Revision-0

Cell Qualification A Performance Metric-Based Approach

Boryann Liaw, Yulun Zhang, Qiang Wang, Shrikant C. Nagpure, Eric J Dufek, Charles C Dickerson

July 2020

The INL is a U.S. Department of Energy National Laboratory
operated by Battelle Energy Alliance

INL/JOU-20-57168-Revision-0

Cell Qualification A Performance Metric-Based Approach

Boryann Liaw, Yulun Zhang, Qiang Wang, Shrikant C. Nagpure, Eric J Dufek, Charles C Dickerson

July 2020

Idaho National Laboratory
Idaho Falls, Idaho 83415

http://www.inl.gov

Prepared for the
U.S. Department of Energy
Office of Energy Efficiency and Renewable Energy, Office of Nuclear Energy
Under DOE Idaho Operations Office
Contract DE-AC07-05ID14517, DE-AC07-05ID14517

Cell Degradation Quantification—A Performance Metric-Based Approach

Yulun Zhang, Qiang Wang, Boryann Liaw*, Shrikant C. Nagpure, Eric J. Dufek, Charles C. Dickerson

Energy Storage and Advanced Transportation

Energy and Environmental Science and Technology

Idaho National Laboratory

Idaho Falls, ID 83415, USA

* E-mail: Boryann.liaw@inl.gov; (208) 526-3238.

Keywords: Battery failure analysis; Rechargeable lithium metal batteries; Charge retention; Capacity fade; Failure mode and effect analysis; Battery cell qualification; Battery cell degradation quantification

Significance

A robust, safe battery operation is vital for consumer electronics, electric vehicles, and power grid. To date, the battery performance is evaluated in laboratories with respect to its specification and application by testing, often short of quantitative failure study and analysis before deployment. The qualification of cells is based on criteria against specification and determined by a small set of parameters as indicators of their quality: e.g. cell capacity, rest voltage and internal dc resistance. It is well experienced that even a very consistent build of cells could have diverse fate in failure, rendering such cell qualification method ineffective for safety assessment and risk mitigation. An effective method to afford early fault detection of anomalies in a battery build is needed. Here, we use an electrochemical analytic diagnosis to decipher good, bad and ugly cells of a build through aging conditions to quantify their propensity to eventual failures. This failure mode and effect analysis (FMEA) and quantification can significantly advance cell screening, qualification, early fault detection, and life prediction to improve battery control and management for reliable, safe operations.

Abstract

A safe and reliable battery operation needs effective diagnostic tools. A quantitative failure analysis (FA) to enable cell qualification and quantify its effectiveness for reliable and safe operation of rechargeable Li batteries (RLB) is shown here. The method can identify and quantify potential failure based on the state of charge (SOC) under any operating conditions. A precise and accurate electrochemical analytic diagnosis (eCAD) of 14 rechargeable Li || NMC-622 cells of the same build are used as an example. The FA by eCAD can quantitatively decipher good, bad and ugly cells in cycle aging. The cell qualification is based on thermodynamic SOC, not experimental conditions. The method provides a quantitative failure mode and effect analysis (FMEA) to reveal diverse "dead Li" formation that affects the reversibility of the Li anode and charge retention in the cell. This cell qualification method highlights the potential to improve cell quality for safe operation, with strong implications for early fault detection, FA, risk mitigation, state estimation and life prediction for reliable and safe RLB operations.

Introduction

Significant advancements in the rechargeable Li battery (RLB) technology propel the use of RLB in portable electronic devices, as recognized in the award of the 2019 Nobel Prize in Chemistry.[1] The acceptance of RLB also inspires the electrification of vehicles and energy storage in the utility grid.[2-4] The RLB systems being used in these applications are demanding better performance and pushing the operation envelopes that raises great concerns on reliability and safety.[5-6] Cell qualification faces unprecedented demands for precision and accuracy that challenges the conventional practice today. As RLB system becomes more massive and complicated, RLB cells are placed in various configurations to function as a pack or bank, the consistency in performance in these cells is becoming critical. The rule of selecting compatible cells in such configurations also becomes complicated and challenging. Traditionally, such compatibility is considered in three aspects: capacity, rest voltage and internal resistance of the cells. When the cells are placed in a topology with series and parallel connections, the task of matching capacity, rest voltage and internal resistance among the cells is complicated to optimize performance, reliability and safety of the battery system.[7] Furthermore, the cells will suffer degradation over time with use.[8-9] The degree and rate of such degradation among the cells might be diverse, often difficult to quantify until they fail. Late detection of cell failure could significantly raise reliability and safety concerns.[10-12]

Here we demonstrate a novel approach of using a failure quantification as criteria to assess RLB cell quality. We use a build of 14 Li || $Li_xNi_{0.6}Mn_{0.2}Co_{0.2}O_2$ (NMC-622) coin cells for illustration. Li metal electrode (LME) is the “holy grail” for next generation high energy RLB designs.[13-16] Currently, almost all Li metal RLB designs suffer from short cycle life issues. The failure mechanisms are known for aprotic liquid electrolyte cell designs, primarily due to the

solid electrolyte interphase (SEI) formation, leading to electrolyte consumption and "inactive" or "dead Li" formation (both are root causes in the loss of Li inventory (LLI)) and the associated kinetic problems.[15, 17-20] Using LME RLB cells in this study provides a unique opportunity to exemplify our unique cell qualification concept. To illustrate this concept, we have recently developed a quantitative electrochemical analytic diagnosis (eCAD) method[21] that can accurately and precisely determine the attributes and the amount of capacity loss in LME-based RLB during cycle aging. This method can clearly identify and quantify capacity fade (*QF*) due to (1) the loss of active materials (LAM) and LLI (QF_{LAM} and QF_{LLI}) and (2) the under-utilization of the active materials (UAM) in the electrode due to rate-dependent polarization (QF_{IR}) and kinetic polarization hindrance (KPH and QF_{KPH}). This method offers a thermodynamic state-of-charge (SOC)-based data analytic capability more reliable than any prior techniques, such as the incremental capacity analysis (d*Q*/d*V*) or alike.[9, 20, 22-24] This approach provides the basis for the thermodynamic state determination[25] to yield accurate Li content in the NMC-622 composition and its changes in the cell reaction. Thus, we were able to quantify the thermodynamic attributes of the *QF* (i.e. QF_{LAM} and QF_{LLI}) and separate them from the kinetic ones under the influence of operating conditions (i.e. polarization that results in QF_{IR} and QF_{KPH}). More detailed description of the analytic method and the terminologies used herein are explained in Ref [21] and will not be repeated here.

Fig. 1(a) shows the charge retention results of these 14 Li || NMC-622 coin cells. The test schedule and protocols used in the tests is explained in Supplementary Information and Fig. S1. A few notable aspects should be emphasized herein. (a) These 14 cells are well qualified in the build for consistency in performance in their early life. This is exemplified by their endurance of 25 charge-discharge (C/D) cycles at C/3 without any deviation from a linear charge retention

behavior. They exhibit a tight $Q_{C/3}$ capacity distribution of 189.09 ± 0.81 mAh g^{-1} (± 0.43%) at Cycle 1 and 177.71 ± 0.77 mAh g^{-1} (± 0.43%) at Cycle 25 with an averaged capacity fade rate of 0.47 mAh g^{-1} $cycle^{-1}$. (b) Upon performing the reference performance test RPT-1 at C/10 and C/20 respectively to determine the charge retention at lower rates, the capacity distribution was slightly widened. At C/10, the standard deviation increased to ± 0.70%, and at C/20 to ± 0.61%. (c) In the subsequent 25 cycles of aging, the 14 cells began to exhibit a diverse charge retention behavior. Cell #8 and #10 showed much shortened cycle life, noted as "ugly" cells. Cell #2, #3, #4, #6 and #13 are "bad" cells, exhibiting accelerated (non-linear) *QF* and falling outside the ± 2σ bounds of 95% confidence interval projected from the $Q_{C/3}$ distribution at Cycle 26 with 0.47 mAh g^{-1} $cycle^{-1}$ fade rate and standard deviation of 1σ = ± 0.54%. (See Fig. 1(b))

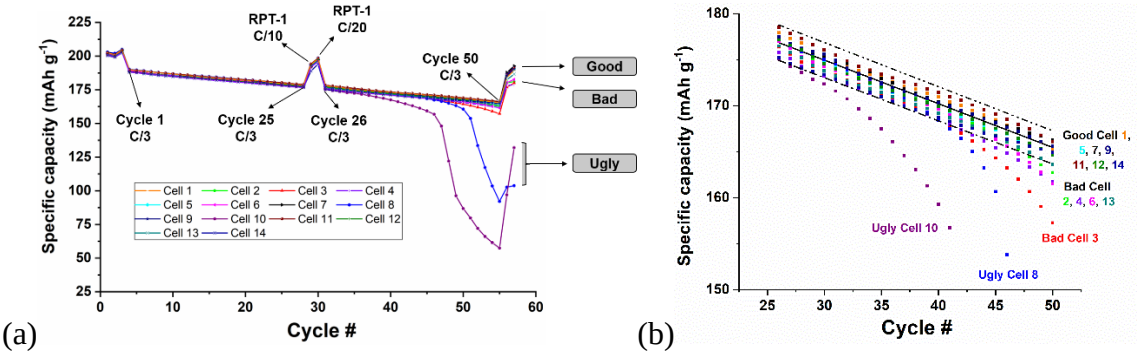

(a) (b)

Fig. 1. (a) Charge retention behavior of a build of 14 Li || NMC-622 coin cells that can be identified as "good," "bad" and "ugly" classes. (b) The criterion of 95% confidence in specific capacity distribution from cycle to cycle (from Cycle 26 to 50 at C/3) in the "good" class, separating it from "bad" and "ugly" ones.

Similar capacity distributions and *QF* behaviors in charge retention are constantly observed in experiments by us and by others, but the origins of such distributions are hardly analyzed and explained quantitatively in the past.[18-19, 26-30] Here, we seize this opportunity to analyze such a behavior using a reliable and quantitative failure mode and effect analysis (FMEA) by eCAD to

gain more insightful understanding of cell failure. Through this practice, we would like to show a better way to quantify failure effects in order to advance practical cell design and manufacturing and to manage risks toward better reliability and safety. As examples, the charge retention and *QF* behavior of three representative cells in the good, bad, and ugly classes are analyzed (in the beginning of life.

Table 1 and Fig. 2) and explained to illustrate the merit of applying this eCAD in a performance-based cell qualification and FMEA.

Qualification of Good, Bad, and Ugly Cells through eCAD-Based FMEA

Fig. 2(a) shows the charge retention behavior of three representative cells (one from each of the good, bad and ugly classes: Cell #7—good, Cell #3—bad, and Cell #8—ugly). Fig. 2(b)-(d) exhibited the eCAD-based analytic discharge curves (along with the corresponding experimental discharge curves at C/3 in the insets) for FMEA. These analytic discharge curves revealed very diverse behaviors in the charge retention and cycle life. At Cycle 25, Fig. 2(a) showed that the three cells behaved quite consistently in the charge retention during the first 25 cycles of aging at C/3. Using the eCAD-based analytic discharge curve of Cell #7 as an example, Fig. 2(b) showed that when SOC>30%, the cell $V_{IR\text{-}free}$ was closely aligned with the *pseudo*-OCV as a function of SOC. Thus, the portion of the eCAD-based analytic discharge curve (i.e. the $V_{IR\text{-}free}$ *vs*. SOC curve) was closely aligned with the universal *pseudo*-OCV *vs*. SOC curve above 30% SOC. This observation indicates that from the beginning of discharge (BOD) to near 30% SOC, the reaction kinetic pathway continues to follow the one defined by the thermodynamics. Only when the cell

reached below 30% SOC, additional polarization-induced effect began to set them apart—this is the so-called "KPH effect" beyond the IR polarization in this article.

With careful examinations, we also noticed that certain differences in the KPH effect were already being revealed in Cell #3 (bad) and Cell #8 (ugly) by eCAD, as highlighted by the gold-colored circular marker in Fig. 2(b). The separation of $V_{IR\text{-}free}$ and *pseudo*-OCV occurred at a higher SOC than 30% SOC (likely near 40% SOC) in both cases. The early detection of such disparity in the KPH effect, even though quite subtle but noticeable, could be beneficial for cell qualification screening in the cell production and battery system integration. The corresponding dQ/dV plots of the good, bad and ugly cells (as shown in Fig. S2 in the Supporting Information) further help visualize the onset and impact of the KPH effect.

At Cycle 45, as the charge retention showed more noticeable differences among the three, the eCAD-based analytic discharge curves revealed how they depart (as Fig. 2(c) highlighted). Here, Cell #7 continued to follow the same linear *QF* progression in charge retention, whereas Cells #3 and #8 began to exhibit non-linearity (as shown in Fig. 2(a)). Comparing Fig. 2(b) and (c), the KPH effect in Cell #7 continued to grow in magnitude (in other words, the NMC-622 capacity continued to be progressively under-utilized) and the onset of the departure of $V_{IR\text{-}free}$ from *pseudo*-OCV occur at a higher SOC cycle by cycle (at Cycle 45, this onset of the separation of $V_{IR\text{-}free}$ and *pseudo*-OCV is roughly around 40% SOC versus 30% at Cycle 25).

In contrast, the eCAD-based analytic discharge curves of Cells #3 and #8 showed a different behavior from that of Cell #7, as highlighted in Fig. 2(c). Both cells showed an early departure of $V_{IR\text{-}free}$ from *pseudo*-OCV from BOD. Furthermore, the separation between $V_{IR\text{-}free}$ and *pseudo*-OCV increased with depth of discharge (DOD). Such a behavior is different from the KPH effect observed in Cycle 25 (Fig. 2(b)). There is no reason to assert that this progressively increasing

separation between $V_{IR\text{-}free}$ and *pseudo*-OCV in polarization as a function of DOD is due to NMC active material or its deterioration in reaction kinetics (activity). It is because the NMC in the seven good cells has behaved consistently very stable. This effect was also recurring cycle by cycle starting at BOD (whereas the SOC at BOC varies from cycle to cycle to a slightly lower SOC). No literature to date has reported such kind of kinetic retardation of NMC activity during cycle aging (that is recurring). In our analysis, the amount of QF_{LAM} is insignificant to create this effect. As this effect was recurring and it became worse cycle by cycle, we thus suspect that this increasing polarization with DOD could only come from the LME anode.

At Cycle 50, the onset of the separation of $V_{IR\text{-}free}$ and *pseudo*-OCV in Cell #7 has been increased to about 45% SOC, as revealed in Fig. 2(d). Cell #3 exhibited a growing impact from the polarization increase at LME, even though the capacity did not suffer a significant loss, compared to that of Cell #7. The most serious degradation was found in Cell #8, which suffered a substantial *QF* that seems much beyond the degree anticipated from the KPH effect. In other words, the drastic increase in *QF* in Cell #8 from Cycle 45 to 50 is quite disproportional to the increase of LME polarization with DOD (i.e. if one followed the same trend as projected from Cells #7 and #3). Therefore, we suspect that the dramatic *QF* around 45% SOC is likely the result of shortage in Li inventory, not just LME polarization. The failure of Cell #8 reveals the transition of failure modes from increasing LME polarization to the shortage of Li inventory. Unarguably, the presumption of a sustainable integrity with NMC with cycle aging helped us to identify the issues with the LME anode.

Interestingly, the failure at the LME from the increasing polarization with DOD and with cycle number to the shortage of Li inventory could be further supported by the evidence in the

SEM micrographs obtained from the spent LME of these three cells at the end of RPT-2 when the cells were fully discharged, as shown in Fig. 3.

Fig. 3(a) shows a representative surface morphology of Cell #7 spent LME anode. Here, reversible Li stripping and deposition is key to the excellent charge retention in the good cells. Such reversibility is suggested by the presence of the smooth surface of the Li grains in LME. However, in certain parts of the LME (as highlighted), some "inactive" or "dead Li" pieces were also found. This is evident by the surface charging effect (brighter contrast) by the e-beam, due to the presence of thicker SEI (known to be electronically insulating layer) on these "dead Li" pieces. The "tortuous" surface of these "dead Li" pieces also suggests that they were likely created by pitting due to uneven Li stripping and current density distribution.[17-18] As cycle aging continues, the amount of "dead Li" continues to grow and accumulate on the surface of LME. Meanwhile, the active surface area available for Li stripping could be reduced as a consequence. This mechanism may induce further increase in unevenness of current density distribution and stripping. Such a vicious cycle in the evolution of the surface morphology, accompanied with increasingly more strenuous Li deposition and stripping, lead to the non-linear *QF* in the bad cells and the resulting surface morphology on the spent LME as shown in Fig. 3(b). At this stage, strips of "dead Li" now cover the surface, leaving voids (where Li was stripped away for the intercalation in the NMC) going deeper into the LME bulk like trenches. In Fig. 3(c), the spent LME of the ugly cell is now packed with a substantial portion of "dead Li" on the surface, whereas the proportion of the voids where active Li was stripped away is much reduced. Thus, the disproportional amount of void space left behind by Li stripping on the spent LME at the end of discharge suggests the amount of active Li is very limited for intercalation as evident by the serious capacity fade.

The implications from these SEM micrographs corroborate our suspicion on the LME performance and its impact on charge retention. Preferential Li stripping resulted in a diverse, unpredictable supply of active Li that created significant variability in charge retention and cycle life among the cells in the same build, even though they behaved quite consistently in the beginning of life.

Table 1. Detailed quantification of capacity fade (*QF*) attributes from the quantitative eCAD-based FMEA for the representative good, bad and ugly cells in the discharge regime. All *Q* and *QF* are expressed in mAh g^{-1}.

Cycle	**Capacity, *Q***	QF_{LAM}	QF_{IR}	QF_{KPH}
Good, Cell 7 [21]				
RPT-0 (C/20)	204.52	0.00	—	—
Cycle 1	189.90	0.26	14.36	0.00
Cycle 5	187.61	1.32	14.36	1.24
Cycle 10	185.31	2.64	14.36	2.21
Cycle 15	183.02	3.97	14.36	3.18
Cycle 20	180.81	5.29	14.36	4.07
Cycle 25	178.51	6.61	14.36	5.04
RPT-1 (C/20)	197.38	7.14	—	—
Cycle 26	177.15	7.32	14.36	5.70
Cycle 30	175.28	8.02	14.36	6.86
Cycle 35	172.99	8.90	14.36	8.28
Cycle 40	170.44	9.78	14.36	9.95
Cycle 45	168.23	10.67	14.36	11.27
Cycle 50	166.27	11.55	14.36	12.35
RPT-2 (C/20)	192.62	11.90	—	—
Bad, Cell 3				
RPT0 (C/20)	203.16	0.00	—	—
Cycle 1	188.63	0.26	14.27	0.00
Cycle 5	186.50	1.13	14.27	1.26
Cycle 10	183.95	2.27	14.27	2.67
Cycle 15	181.74	3.40	14.27	3.75
Cycle 20	179.53	4.53	14.27	4.83
Cycle 25	177.15	5.67	14.27	6.07
RPT-1 (C/20)	197.04	6.12	—	—
Cycle 26	176.39	6.30	14.27	6.21
Cycle 30	173.84	7.02	14.27	8.04
Cycle 35	171.37	7.92	14.27	9.60
Cycle 40	168.57	8.82	14.27	10.98

Cycle 45	164.31	9.72	14.27	12.32
Cycle 50	157.26	10.62	14.27	13.66
RPT-2 (C/20)	180.04	10.98	—	—
Ugly, Cell 8				
RPT-0 (C/20)	203.67	0.00	—	—
Cycle 1	191.18	0.26	12.23	0.00
Cycle 5	187.86	0.94	12.23	2.64
Cycle 10	185.57	1.89	12.23	3.99
Cycle 15	183.36	2.83	12.23	5.25
Cycle 20	181.06	3.78	12.23	6.60
Cycle 25	178.68	4.72	12.23	8.04
RPT-1 (C/20)	198.57	5.10	—	—
Cycle 26	177.49	5.28	12.23	8.67
Cycle 30	175.03	6.00	12.23	10.42
Cycle 35	172.22	6.90	12.23	12.32
Cycle 40	168.40	7.80	12.23	13.58
Cycle 45	160.66	8.70	12.23	15.24
Cycle 50	92.15	9.60	12.23	16.91
RPT-2 (C/20)	103.79	9.96	—	—

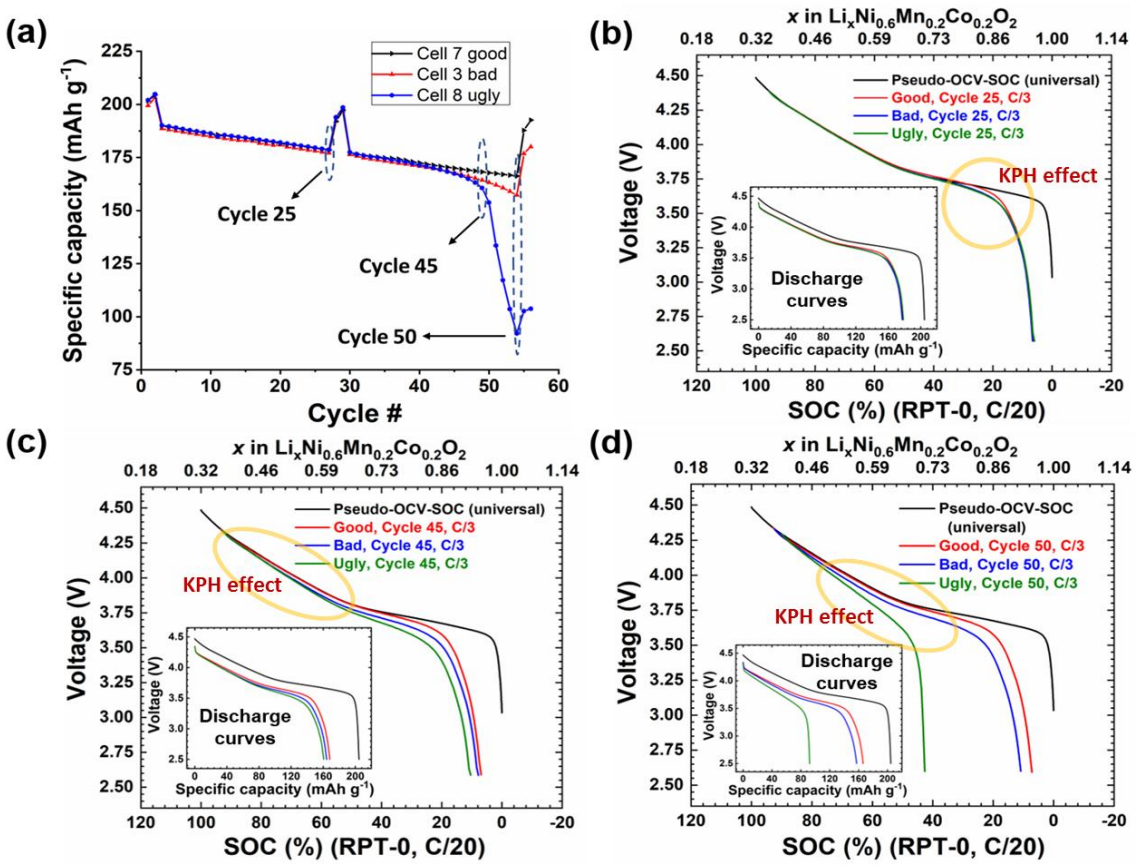

Fig. 2. Failure analyses of the variability in cycle life of three LME || NMC-622 cells: Cell #7 (a "good" cell), Cell #3 (a "bad" cell), and Cell #8 (an "ugly" cell). (a) The charge retention

curves, (b) the eCAD-based analytic discharge curves at Cycle 25, (c) Cycle 45 and (d) Cycle 50 for the three cells. Insets are the experimental discharge curves for comparison. The universal *pseudo-OCV*–SOC curve derived from the averaging of the C/20 charge and discharge curves is shown in black in each plot to provide a baseline for comparison with the change of cell voltage as a function of Li content in the NMC cathode.

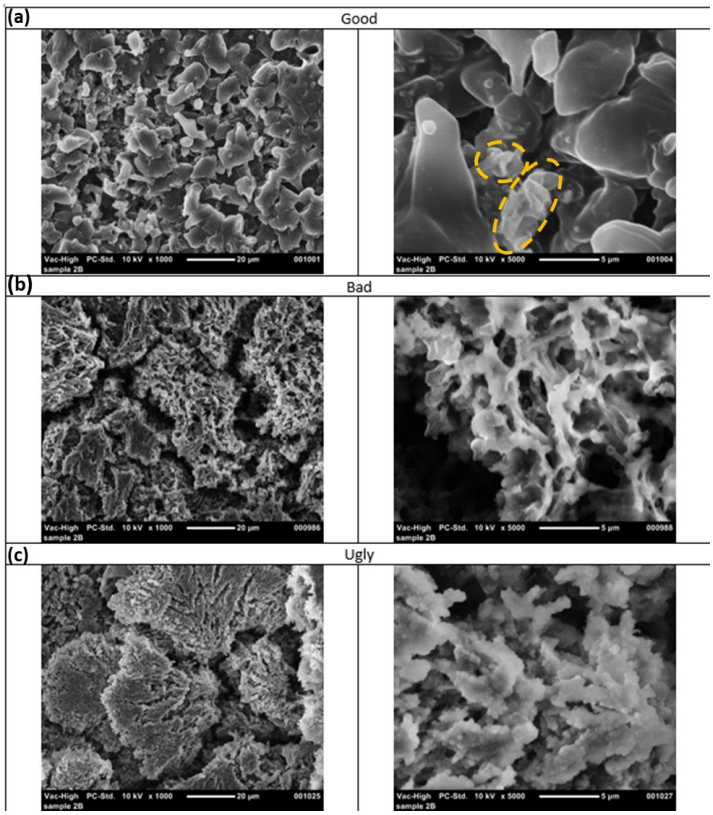

Fig. 3. SEM micrographs showing the morphological changes of the Li anode in Cell #7 (good), Cell #3 (bad) and Cell #8 (ugly) at the end of the cycle aging.

Conclusion

We have shown the charge retention of 14 rechargeable Li || NMC-622 cells of the same build and their classification into good, bad and ugly classes based on performance in cycle aging. Via the illustration of an electrochemical analytic diagnosis (eCAD)-based failure mode and effect analysis (FMEA) on three sample cells, one from each class; we show cell qualification can be reliably achieved by this method based on thermodynamic state of charge (SOC) determination. Precise and accurate quantification of capacity fade (QF) attributes can be achieved. Such quantification can separate (1) the loss of active materials (QF_{LAM})—a thermodynamic attribute—from those that cause under-utilization of the active material (QF_{UAM}) in the electrodes—kinetic attributes—due to (2) reduction in capacity (QF_{IR}) by rate-dependent, IR-induced polarization and (3) deterioration from kinetic polarization hindrance (QF_{KPH}). We found very consistent, well-behaving Li metal cells in the same build could exhibit very diverse charge retention and cycle life results. Such a significant diversity and variability in cycle life is a result of uneven, preferential Li stripping, “dead Li” formation and surface morphology evolution on Li metal electrode (LME) in cycle aging as revealed by eCAD-based FMEA and SEM micrographs of the spent LME at the end of cycle aging in these cells. The interplay of these phenomena resulted in a diverse distribution of Li inventory that greatly affects charge retention and cycle life during cycle aging. Using this quantitative eCAD-based FMEA, we demonstrated a unique cell qualification method that has not been reported before.

Acknowledgements

This work has been partially supported by the Assistant Secretary for Energy Efficiency and Renewable Energy, Office of Vehicle Technologies of the U.S. Department of Energy through

the Advanced Battery Materials Research (BMR) Program (Battery500 Consortium). Idaho National Laboratory is operated by Battelle Energy Alliance under Contract Nos. DE-AC07-05ID14517 for the U.S. Department of Energy. The United States Government retains and the publisher, by accepting the article for publication, acknowledges that the United States Government retains a nonexclusive, paid-up, irrevocable, world-wide license to publish or reproduce the published form of this manuscript, or allow others to do so, for United States Government purposes. The data analytics part of the work has been partially supported by the Laboratory Directed Research and Development (LDRD) program at INL (Project No.: 19P45-013FP). The authors would like to thank the Cell Analysis, Modeling and Prototyping (CAMP) facility at Argonne National Laboratory (ANL) for providing the cathode laminates used in this work.

Author Contributions

BL developed the concept for this work. BL led the data analysis. YZ and QW analyzed the data. YZ and BL developed the FMEA. EJD, SCN, and CCD developed the test protocols and procedures and conducted the experiments and cell testing.

Declaration of Interests

The authors declare no competing interests.

References:

1. Li, M.; Lu, J.; Chen, Z.; Amine, K., 30 Years of lithium-ion batteries. *Adv. Mater.* **2018,** *30* (33), 1800561.

2. Lu, L.; Han, X.; Li, J.; Hua, J.; Ouyang, M., A review on the key issues for lithium-ion battery management in electric vehicles. *J. Power Sources* **2013,** *226*, 272-288.
3. Dunn, B.; Kamath, H.; Tarascon, J.-M., Electrical energy storage for the grid: A battery of choices. *Science* **2011,** *334* (6058), 928-935.
4. Barré, A.; Deguilhem, B.; Grolleau, S.; Gérard, M.; Suard, F.; Riu, D., A review on lithium-ion battery ageing mechanisms and estimations for automotive applications. *J. Power Sources* **2013,** *241*, 680-689.
5. Abada, S.; Marlair, G.; Lecocq, A.; Petit, M.; Sauvant-Moynot, V.; Huet, F., Safety focused modeling of lithium-ion batteries: A review. *J. Power Sources* **2016,** *306*, 178-192.
6. Williard, N.; He, W.; Hendricks, C.; Pecht, M., Lessons learned from the 787 Dreamliner issue on lithium-ion battery reliability. *Energies* **2013,** *6* (9), 4682-4695.
7. Dubarry, M.; Truchot, C.; Devie, A.; Liaw, B. Y., State-of-charge determination in lithium-ion battery packs based on two-point measurements in life. *J. Electrochem. Soc.* **2015,** *162* (6), A877-A884.
8. Wang, H.; Frisco, S.; Gottlieb, E.; Yuan, R.; Whitacre, J. F., Capacity degradation in commercial Li-ion cells: The effects of charge protocol and temperature. *J. Power Sources* **2019,** *426*, 67-73.
9. Dubarry, M.; Svoboda, V.; Hwu, R.; Liaw, B. Y., Incremental Capacity Analysis and Close-to-Equilibrium OCV Measurements to Quantify Capacity Fade in Commercial Rechargeable Lithium Batteries. *ECS Solid State Lett.* **2006,** *9* (10), A454.
10. Santhanagopalan, S.; White, R. E., Quantifying cell-to-cell variations in lithium ion batteries. *Int. J. Electrochem.* **2012,** *2012*.

11. Schuster, S. F.; Brand, M. J.; Berg, P.; Gleissenberger, M.; Jossen, A., Lithium-ion cell-to-cell variation during battery electric vehicle operation. *J. Power Sources* **2015,** *297*, 242-251.
12. Dubarry, M.; Vuillaume, N.; Liaw, B. Y., Origins and accommodation of cell variations in Li-ion battery pack modeling. *Int. J. Energy Res.* **2010,** *34* (2), 216-231.
13. Liu, J.; Bao, Z.; Cui, Y.; Dufek, E. J.; Goodenough, J. B.; Khalifah, P.; Li, Q.; Liaw, B. Y.; Liu, P.; Manthiram, A.; Meng, Y. S.; Subramanian, V. R.; Toney, M. F.; Viswanathan, V. V.; Whittingham, M. S.; Xiao, J.; Xu, W.; Yang, J.; Yang, X.-Q.; Zhang, J.-G., Pathways for practical high-energy long-cycling lithium metal batteries. *Nat. Energy* **2019,** *4* (3), 180-186.
14. Thackeray, M. M.; Wolverton, C.; Isaacs, E. D., Electrical energy storage for transportation—approaching the limits of, and going beyond, lithium-ion batteries. *Energy Environ. Sci.* **2012,** *5* (7), 7854-7863.
15. Niu, C.; Pan, H.; Xu, W.; Xiao, J.; Zhang, J.-G.; Luo, L.; Wang, C.; Mei, D.; Meng, J.; Wang, X.; Liu, Z.; Mai, L.; Liu, J., Self-smoothing anode for achieving high-energy lithium metal batteries under realistic conditions. *Nat. Nanotechnol.* **2019,** *14* (6), 594-601.
16. Niu, C.; Lee, H.; Chen, S.; Li, Q.; Du, J.; Xu, W.; Zhang, J.-G.; Whittingham, M. S.; Xiao, J.; Liu, J., High-energy lithium metal pouch cells with limited anode swelling and long stable cycles. *Nat. Energy* **2019,** *4* (7), 551-559.
17. Aurbach, D.; Zinigrad, E.; Cohen, Y.; Teller, H., A short review of failure mechanisms of lithium metal and lithiated graphite anodes in liquid electrolyte solutions. *Solid State Ionics* **2002,** *148* (3), 405-416.
18. Nagasaki, M.; Nishikawa, K.; Kanamura, K., Deterioration analysis of lithium metal anode in full cell during long-term cycles. *J. Electrochem. Soc.* **2019,** *166* (12), A2618-A2628.

19. Wang, Y.; Fu, L.; Shi, L.; Wang, Z.; Zhu, J.; Zhao, Y.; Yuan, S., Gel polymer electrolyte with high Li^+ transference number enhancing the cycling stability of lithium anodes. *ACS Appl. Mater. Interfaces* **2019,** *11* (5), 5168-5175.
20. Chen, K.-H.; Wood, K. N.; Kazyak, E.; LePage, W. S.; Davis, A. L.; Sanchez, A. J.; Dasgupta, N. P., Dead lithium: mass transport effects on voltage, capacity, and failure of lithium metal anodes. *J. Mater. Chem. A* **2017,** *5* (23), 11671-11681.
21. Zhang, Y.; Wang, Q.; Liaw, B.; Nagpure, S. C.; Dufek, E. J.; Dickerson, C. C., A quantitative failure analysis on capacity fade in rechargeable lithium metal cells. *J. Electrochem. Soc.* **2020**, 167, 090502.
22. Dubarry, M.; Svoboda, V.; Hwu, R.; Liaw, B. Y., Capacity loss in rechargeable lithium cells during cycle life testing: The importance of determining state-of-charge. *J. Power Sources* **2007,** *174* (2), 1121-1125.
23. Dubarry, M.; Liaw, B. Y., Identify capacity fading mechanism in a commercial $LiFePO_4$ cell. *J. Power Sources* **2009,** *194* (1), 541-549.
24. Truchot, C.; Dubarry, M.; Liaw, B. Y., State-of-charge estimation and uncertainty for lithium-ion battery strings. *Appl. Energy* **2014,** *119*, 218-227.
25. Li, Z.; Huang, J.; Liaw, B. Y.; Zhang, J., On state-of-charge determination for lithium-ion batteries. *J. Power Sources* **2017,** *348*, 281-301.
26. Liu, M.; Cheng, Z.; Qian, K.; Verhallen, T.; Wang, C.; Wagemaker, M., Efficient Li-metal plating/stripping in carbonate electrolytes using a $LiNO_3$-gel polymer electrolyte, monitored by operando neutron depth profiling. *Chem. Mater.* **2019,** *31* (12), 4564-4574.
27. Hao, F.; Verma, A.; Mukherjee, P. P., Electrodeposition stability of metal electrodes. *Energy Storage Mater.* **2019,** *20*, 1-6.

28. Aryanfar, A.; Brooks, D. J.; Colussi, A. J.; Hoffmann, M. R., Quantifying the dependence of dead lithium losses on the cycling period in lithium metal batteries. *Phys. Chem. Chem. Phys.* **2014,** *16* (45), 24965-24970.

29. Steiger, J.; Kramer, D.; Mönig, R., Microscopic observations of the formation, growth and shrinkage of lithium moss during electrodeposition and dissolution. *Electrochim. Acta* **2014,** *136*, 529-536.

30. Liaw, B. Y.; Wang, F.; Wei, Y., MANAGING SAFETY RISK BY CELL MANUFACTURERS. *Electrochemical Power Sources: Fundamentals, Systems, and Applications: Li-Battery Safety* **2018**, *Chapter 8A.1*, 269-302.